DIFFERENT TYPES OF X-RAY BURSTS FROM GRS 1915+105 AND THEIR ORIGIN

J. S. YADAV,[1] A. R. RAO,[2] P. C. AGRAWAL,[3] AND B. PAUL[4]

Tata Institute of Fundamental Research, Homi Bhabha Road, Mumbai 400 005, India

AND

S. SEETHA,[5] AND K. KASTURIRANGAN

ISRO Satellite Centre, Airport Road, Vimanpura P.O. Bangalore 560 017, India

ABSTRACT

We report X-ray observations of the Galactic X-ray transient source GRS 1915+105 with the pointed proportional counters of the Indian X-ray Astronomy Experiment (IXAE) onboard the Indian satellite *IRS-P3*, which show remarkable richness in temporal variability. The observations were carried out on 1997 June 12–29 and August 7–10, in the energy range of 2–18 keV and revealed the presence of very intense X-ray bursts. All the observed bursts have a slow exponential rise, a sharp linear decay, and broadly can be put in two classes: irregular and quasi-regular bursts in one class, and regular bursts in the other. The regular bursts are found to have two distinct timescales and to persist over extended durations. There is a strong correlation between the preceding quiescent time and the burst duration for the quasi-regular and irregular bursts. No such correlation is found for the regular bursts. The ratio of average flux during the burst time to the average flux during the quiescent phase is high and variable for the quasi-regular and irregular bursts, while it is low and constant for the regular bursts. We present a comprehensive picture of the various types of bursts observed in GRS 1915+105 in the light of the recent theories of advective accretion disks. We suggest that the peculiar bursts that we have seen are characteristic of the change of state of the source. The source can switch back and forth between the low-hard state and the high-soft state near critical accretion rates in a very short timescale, giving rise to the irregular and quasi-regular bursts. The fast timescale for the transition of the state is explained by invoking the appearance and disappearance of the advective disk in its viscous timescale. The periodicity of the regular bursts is explained by matching the viscous timescale with the cooling timescale of the postshock region. A test of the model is presented using the publicly available 13–60 keV *RXTE*/PCA data for irregular and regular bursts concurrent with our observations. It is found that the 13–60 keV flux relative to the 2–13 keV flux shows clear evidence for state change between the quiescent phase and the burst phase. The value of this ratio during burst is consistent with the values observed during the high-soft state seen on 1997 August 19, while its value during quiescent phase is consistent with the values observed during the low-hard state seen on 1997 May 8.

Subject headings: accretion, accretion disks — binaries: close — black hole physics — stars: individual (GRS 1915+105) — X-rays: bursts — X-rays: stars

1. INTRODUCTION

The X-ray transient source GRS 1915+105 was discovered in 1992 with the WATCH all sky X-ray monitor onboard the *GRANAT* satellite (Castro-Tirado et al. 1994). Superluminal motions of two symmetric radio-emitting jets of GRS 1915+105 were discovered by Mirabel & Rodriguez (1994). Several features in the observed properties of GRS 1915+105, such as the power density spectra (PDS) with the quasi-periodic oscillation (QPO) feature, a hard X-ray tail, and the subsecond time variability are typical characteristics of black hole binaries. The X-ray intensity is found to be more than 10^{39} ergs s^{-1} (based on an assumed distance of 12.5 kpc) for extended periods, which is super-Eddington luminosity for a neutron star (Mirabel & Rodriguez 1994). The other Galactic source of superluminal jets, GRO J1655−40, has been shown to harbor a compact object of mass $\sim 7\ M_\odot$ (Orosz & Bailyn 1997). The combination of relativistic jets and a central black hole has

earned these two objects the name "microquasars," as they seem to be stellar mass analogs of the massive black hole systems in quasars and other active galactic nuclei (AGNs). These microquasars have opened the possibility of studying phenomena in our Galaxy that until recently were believed to be restricted to distant quasars and a few AGNs. In particular, it has been realized that since the characteristic dynamic times in the flow of matter onto a black hole are proportional to its mass, events with intervals of minutes in a microquasar could correspond to analogous phenomena with duration of thousands of years in a quasar of $10^9\ M_\odot$.

GRS 1915+105 was observed to be X-ray active in 1994 using BATSE instrument. The source went into a very high X-ray intensity state in early 1996 and was observed on several occasions by the pointed proportional counters (PPCs) of the Indian X-ray Astronomy Experiment (IXAE) (Agrawal et al. 1997; Paul et al. 1997), the proportional counter array (PCA), and the all sky monitor (ASM) of the *Rossi X-Ray Timing Explorer* (*RXTE*) (Bradt 1996). The X-ray intensity was found to vary on a variety of timescales and the light curve showed a complicated pattern of dips and rapid transitions between high and low intensity (Greiner, Morgan, Remillard 1996; Belloni et al. 1997b; Taam, Chen, & Swank 1997). PPC observations of

---

[1] jsyadav@tifr.res.in.
[2] arrao@tifr.res.in.
[3] pagrawal@tifr.res.in.
[4] bpaul@tifr.res.in.
[5] seetha@isac.ernet.in.

TABLE 1
THE GRS 1915+105 OBSERVATIONS BY IXAE DURING 1997 JUNE–AUGUST

Day of Year	Date	Start time	End time	Orbits	Time(s)	Mode	PPC
164	Jun 12	17:36:57	19:27:24	2	1600	M	1 2 3
168	Jun 16	14:21:46	18:04:10	4	1880	M	1 2 3
169	Jun 17	13:59:54	17:42:50	3	2760	M	– 2 3
169	Jun 18	11:55:40	15:40:19	3	1630	M	– 2 3
170	Jun 19	11:35:54	15:20:26	3	1530	M	1 2 3
173	Jun 21	10:59:28	17:55:38	5	5070	N	1 2 3
174	Jun 22	12:12:24	19:20:50	5	5300	N	1 2 3
175	Jun 23	11:52:08	18:59:46	5	5400	N	1 2 3
176	Jun 24	11:30:15	18:38:52	5	5700	N	1 2 3
177	Jun 25	11:12:05	18:18:02	5	5700	N	1 2 3
178	Jun 26	10:50:03	17:56:00	5	5220	N	1 2 3
179	Jun 27	15:30:57	17:34:22	3	2770	M	– 2 3
181	Jun 29	11:27:23	15:11:55	3	2490	M	– 3
220	Aug 07	11:25:19	18:37:51	5	5750	N	1 2 3
221	Aug 08	10:05:49	17:17:19	5	4740	N	1 2 3
222	Aug 09	10:49:03	17:52:31	5	4850	N	1 2 3
223	Aug 10	12:13:19	19:16:15	5	5360	N	1 2 3

NOTE.—M = medium mode, N = Nominal mode.

GRS 1915+105 in its low-hard state in 1996 July showed intensity variations of a factor of 2–3 at a 100–400 ms time-scale (Paul et al. 1997, 1998a). Strong (rms variability 9%) and narrow ($v/\delta v \approx 5$) QPOs of varying frequency were discovered in GRS 1915+105 with the PPC observations (Agrawal et al. 1996). Quasi-regular X-ray and infrared flares with a spacing of ~30 minutes, were observed during simultaneous X-ray/IR observations (Eikenberry et al. 1998). These observations suggest that IR flares are signatures of plasma ejection in the inner part of the accretion disk, and they that are called "baby jets" in analogy to the much larger superluminal ejection events. At later times, the X-ray flares decouple from IR flares, ruling out thermal reprocessing of the X-rays as the source of the IR flares. Other simultaneous observations of GRS 1915+105 in the X-ray, IR, and radio wavelengths confirm that the IR and radio flares are associated with the X-ray dips (Mirabel et al. 1998).

The most compelling evidence for the existence of a black hole in Galactic X-ray binaries normally comes from the measured mass function, which indicates that the mass of the compact object is much larger than that permitted for a neutron star. In the absence of measured binary parameters (like in the case of GRS 1915+105), phenomenological arguments are normally used, which, though compelling for a class of objects, are not conclusive enough for individual cases. This is mainly because the accretion disk around a black hole has properties quite similar to that around a low magnetic field neutron star (Tanaka & Lewin 1995). Recent progress in the understanding of accretion onto black holes has suggested that the black hole accretion disks are cooled by advection in their innermost parts (Chakrabarti 1996a; Abramowicz & Percival 1997; Narayan, Mahadevan, & Quataert 1998). Based on the new accretion theories involving advection, features in black hole accretion that uniquely distinguish them from low magnetic field accreting neutron stars have been identified. Narayan et al. (1997a) have argued that advective cooling can occur throughout the disk for black hole accretion, providing a unique way of identifying black hole binaries in their quiescent state. Chakrabarti & Titarchuk (1995) have argued that in the

very high state of the sources, black hole binaries should have a unique extended power law owing to bulk Comptonization (see also Laurent & Titarchuk 1999). In an earlier paper (Paul et al. 1998b), we presented possible evidence for the direct detection of advection in GRS 1915+105. This is based on the detection of regular and persistent X-ray bursts that have a slow exponential rise, sharp decay, and hardening of the spectrum as the burst progresses.

In this paper, we present a detailed analysis of all the IXAE observations of GRS 1915+105 during 1997 June–August. We specially study temporal variations on a time-scale from few seconds to few minutes. In the following sections, we describe the observations and the properties of 1889 bursts observed with PPCs. We discuss our results in the framework of advective accretion disk models.

2. OBSERVATIONS

IXAE, onboard the Indian satellite *IRS-P3*, consists of three identical PPCs and one X-ray sky monitor and it was launched on 1996 March 21 from Shriharikota Range, India. The observations were carried out using all three PPCs of IXAE. The PPCs are filled with an argon-methane mixture at 800 torr pressure and have a total area of 1200 cm². The operating energy range is between 2 keV and 18 keV, and a passive collimator restricts the field of view to $2°3 \times 2°3$. The energy resolution is $\approx 22(E/6)^{-1/2}\%$ at E keV with a detection efficiency of about 65% at 6 keV and 10% at 15 keV. Each PPC is a multilayer unit consisting of 54 anode cells of size 1.1×1.1 cm arranged in three identical layers. The end cells of each layer and all the 18 anodes of the third layer are connected together and operated as a veto layer for the top two layers that constitute the X-ray detection volume. The alternate anodes in each of the two X-ray detection layers are joined together and operated in mutual anticoincidence to reject charged particle induced background. Each PPC has its own front-end electronics and a processing electronics. The processing electronics selects the genuine events based on the predetermined logic conditions. An 8086 microprocessor based system handles the data from each PPC and stores them in 4 Mbit of

memory. The data storage is done in different modes, which can be set by commands. For further details of the PPCs and the observation methodology see Rao et al. (1998).

The *IRS-P3* satellite is in a circular orbit at an altitude of 830 km and inclination of 98°. A star tracker onboard is co-aligned with the viewing axes of the proportional counters and used for pointing toward the X-ray sources with a pointing accuracy of about 0°.1. The high inclination and high-altitude orbit is found to be very background-prone, and the useful observation time is limited to the latitude ranges typically from $-30°$ S to $+50°$ N. Further, the South Atlantic Anomaly (SAA) region restricts the observation to about five of the 14 orbits per day. Observations with the PPCs are usually made in the nominal mode (N), with 1.0 s time resolution, in about five orbits of the satellite every day, and each observation has a duration of about 20 minutes. In the medium mode (M), with time resolution of 0.1 s, data are usually available for only three orbits owing to the limited size of the onboard data storage unit. During 17 days of observations from June 12 to August 10, data from 71 orbits were collected and a total of 67,750 s of useful exposure time was obtained. A summary of the observations is given in Table 1.

3. THE BURST PROFILES

Intense X-ray bursts are observed throughout the PPC observations over the period of 1997 June 12–29 and August 7–10. These bursts can broadly be put into two classes: regular bursts lasting typically for a few days and centered around a fixed period with low dispersion ($\delta P/P \sim 5\%$–10%) and irregular bursts with no fixed periodicity ($\delta P/P \geq 50\%$). The period of regular bursts shows two distinct timescales during our observations, and quasi-regular bursts with properties between those observed for the regular and irregular bursts have also been seen. The observed bursts are, therefore, classified into four types: (1) regular bursts having a slow rise and fast decay lasting for ~ 15 s and recurring every 21 s; (2) regular bursts, having a slow rise and sharp decay lasting for ~ 20 s and recurring every 46 s; (3) quasi-regular bursts of variable duration, slow rise and sharp decay; and (4) irregular bursts, with duration of a few tens to a few hundred seconds, followed by sharp decay. Sharp decay is a common feature of all the bursts. All the regular bursts usually have two-peak structure, while quasi-regular and irregular bursts show multipeak structure.

Representative 2–18 keV light curves of 300 s duration, obtained on different days and added for all the PPCs (except on June 27, when only PPCs 2 and 3 were on), are shown in top four panels of Figure 1. These burst profiles were detected independently in each of the PPCs. All the panels in the figure have similar y-axis scales. Regular bursts of ~ 21 s recurrence time were detected August 7–10, with the second peak being prominent and a sharp narrow dip between the two peaks; regular bursts of ~ 46 s recurrence time were detected June 12–17 and again June 22–26, with the first peak being prominent; quasi-irregular bursts were seen June 19–21, and irregular bursts were detected on June 18 and June 27–29. In the second panel (*from bottom*), we show regular bursts observed on 1997 June 22. The time zero corresponds to 1997 June 22, 19:10 UT with the PPCs. Similar burst profiles are seen from publicly available 2–13 keV *RXTE*/PCA data of 1997 June 22, which are shown in
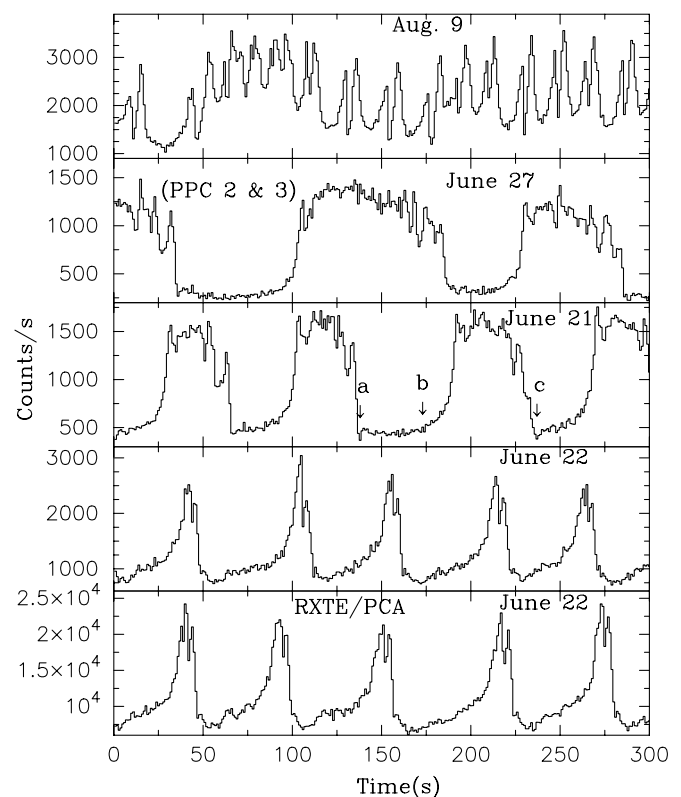

Fig. 1.—Regular bursts with ~ 21 s recurrence time (*first panel from the top*), irregular bursts (*second panel*), quasi-regular bursts (*third panel*), and regular bursts with ~ 46 s recurrence time (*fourth panel*) observed in GRS 1915+105 with all the PPCs (except on June 27 [irregular bursts] when only PPCs 2 and 3 were on). Date of each observation is given in the respective panels. The regular bursts observed by *RXTE*/PCA on June 22 are shown in the bottom panel for comparison with the regular bursts observed on June 22 with the PPCs. See text for details.

the bottom panel of Figure 1. The time zero corresponds to 1997 June 22, 19:35 UT. Remarkable similarity between temporal profiles of regular bursts observed by PPCs and independently by the PCA about 25 minutes later is apparent from the first and second panels (*from the bottom*) of Figure 1. A secondary peak near the end of the bursts is a common feature of all the bursts. The quasi-regular and irregular long bursts show higher variability near the end of the burst, and the burst duration is correlated to the quiescent state period just prior to the burst, which we shall discuss in detail in the next section.

All the bursts start with a well-defined sharp peak and decay faster than they rise. We define a burst event as a full cycle of one quiescent interval followed by one burst. The recurrence time is the sum of quiescent time and the burst duration. With this definition there is no interval between burst events. This defines the individual burst events adequately for the regular and quasi-regular bursts. In the case of irregular bursts, we add the additional criterion that separate events are considered to be only those whose quiescent count rate goes below 250 counts s^{-1} for individual PPC in the total 2.0–18.0 keV energy band. We measured the start of a burst event (corresponding to the end of the previous one) as the time of the small dip at the end of the decay. Since all the bursts start with a sharp peak, the time of the peak can be taken as the separation between the quiescent phase and the burst phase. We have marked the positions in the third panel of Figure 1 for a burst event: the

beginning of the quiescent phase (preceding) is marked by "a," the end of the quiescent phase and start of burst phase is marked by "b," and the end of the burst phase and start of the next quiescent phase (following) is marked by "c." We have detected bursts in all our observations. We have calculated mean recurrence time for each day, and results are shown in Figure 2. The error bar represents one σ variation in the recurrence time during the observations on each day. The large variations on June 18, June 27, and June 29 represent irregular bursts on these days, while small variations on June 12–17, June 22–26, and August 7–10 show regular bursts during these durations. The quasi-regular bursts were observed on June 19 and June 21.

In all the bursts, a dip is present just before the decay of the burst. But the most remarkable feature of our observations is the persistence of the regular bursts for a few days with very similar shape, structure, and period. For both types of regular bursts, the recurrence time for the successive bursts shows a random walk in time instead of any regular pattern. The distribution of burst recurrence time for each day fits well with a Gaussian, with a tail on the higher side, having a width σ of 3–5 s for both the types of regular bursts. In the case of irregular bursts, the distribution of burst recurrence time shows large variations.

To improve the statistical accuracy of the data, we have co-added a large number of bursts by matching the last peak. The co-added burst profiles in two different energy ranges (2–6 keV and 6–18 keV) are shown in the top panels,

while the hardness ratio is shown in the bottom panels of Figures 3a and 3b for all four types of bursts. We chose to align individual burst of the same type to the last peak in order to keep sharp features during the decay of all the bursts, while the sharp features during the rise are smeared out owing to the addition of bursts of different duration, especially in the case of quasi-regular and irregular bursts. Intensity changes are more prominent at higher energy, and the energy spectrum becomes harder as the burst progresses in all types. The burst is hardest near the end of its decay. This is a unique feature of these bursts that distinguishes them from the bursts seen in low-mass X-ray binaries (LMXBs), which become softer in the decaying phase (Lewin, van Paradijs, & Taam 1995).

We show the "rise" and the "decay" segments of the profiles of different types of bursts in Figure 4. We arbitrarily chose the burst start time at 0 s and the burst end time at 40 s for all types of the bursts to highlight the fact that the slow rise and sharp decay is a common feature of all the bursts. The flux is normalized to the start point for the rise segment and to the end point for the decay segment of the burst profile. The "rise" and the "decay" profiles are strikingly similar for both the types of regular bursts observed on August 9 and June 22. A least-squares fit with a function $f(t) = a \times \exp^{[(t-t_0)/t_r]}$ to the rising segment of the burst profile gives time constant $t_r = 10$ s for the regular bursts, while it has a value in the range of 5–6 s for the quasi-regular and irregular bursts. The burst decay is con-
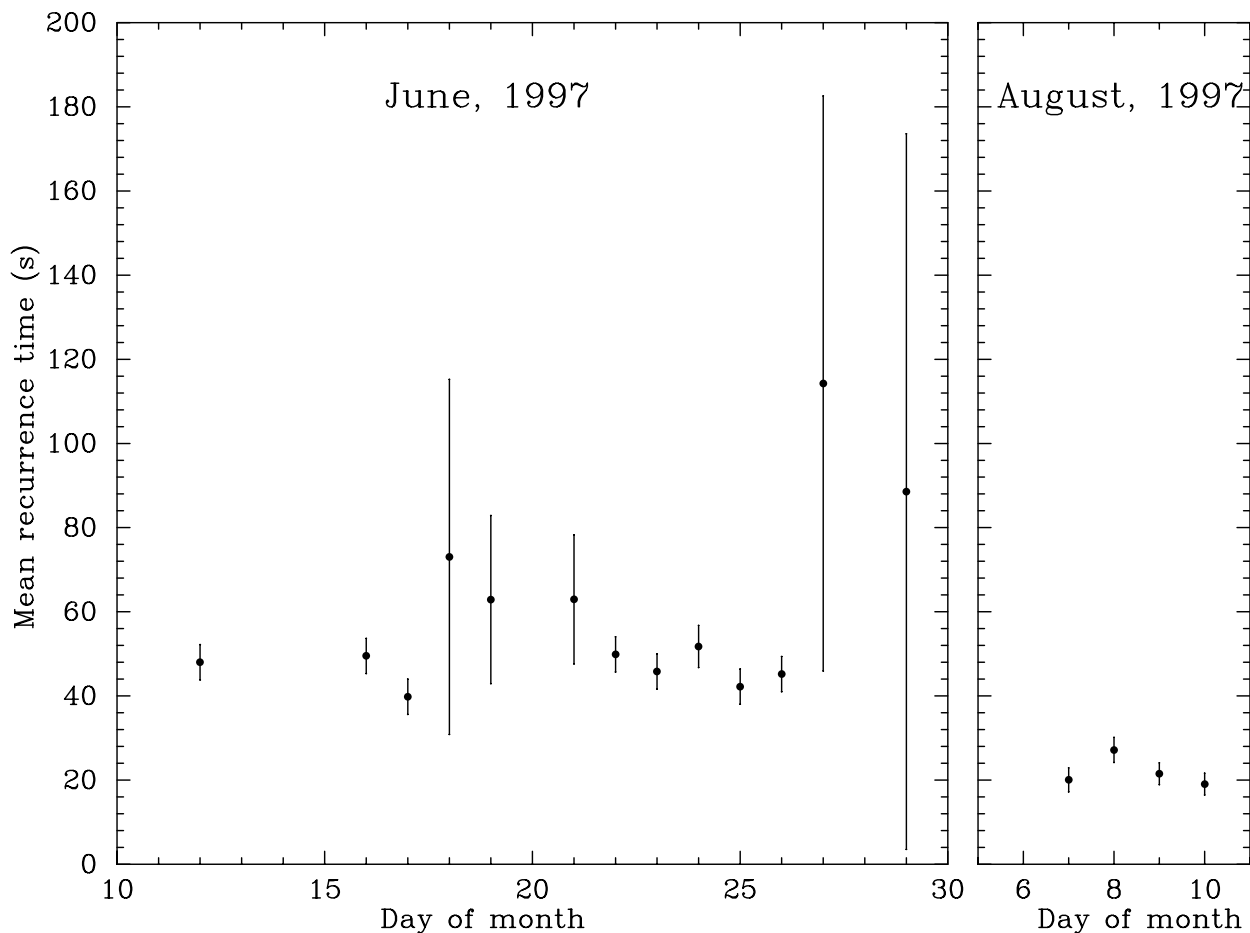

FIG. 2.—Mean burst recurrence time for each day of observation. The error bars show 1 σ variation in each day of observation.
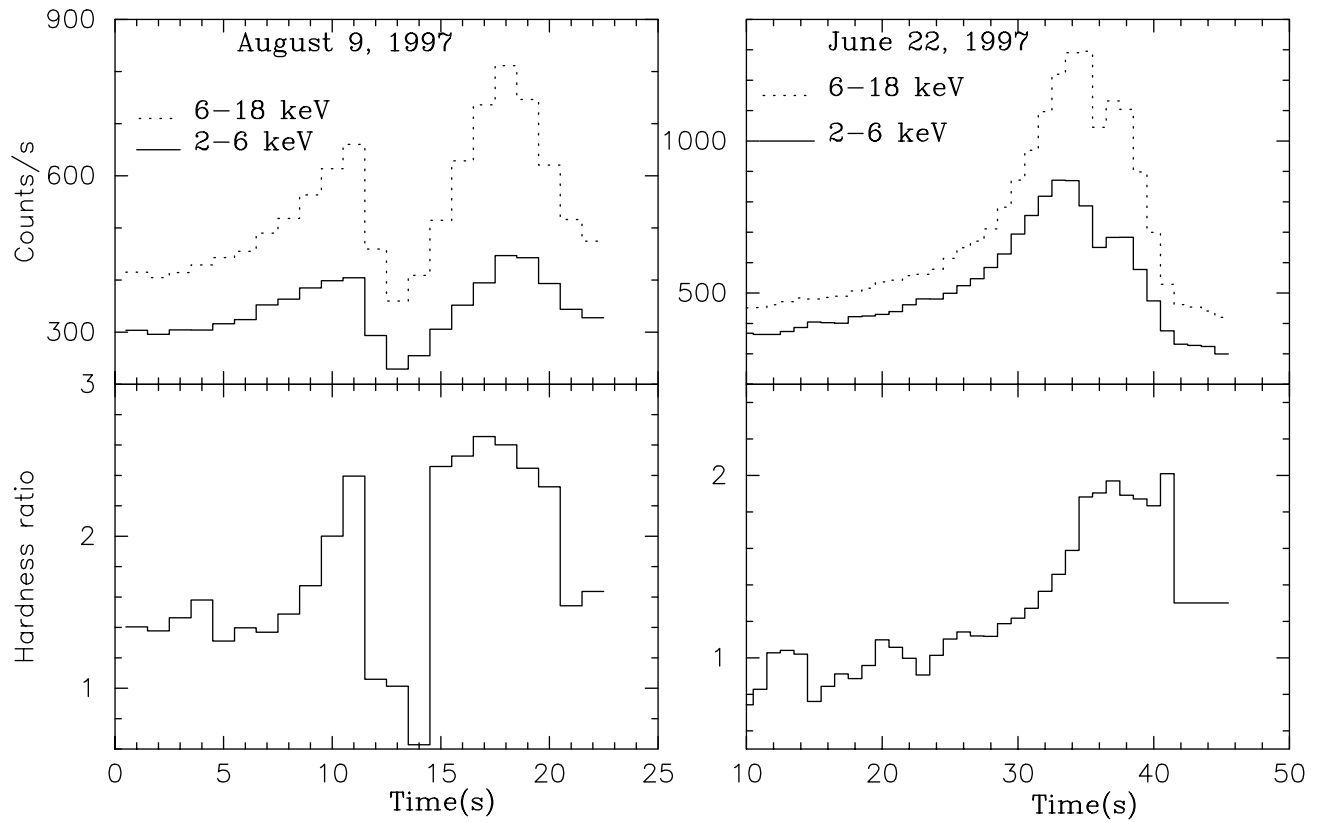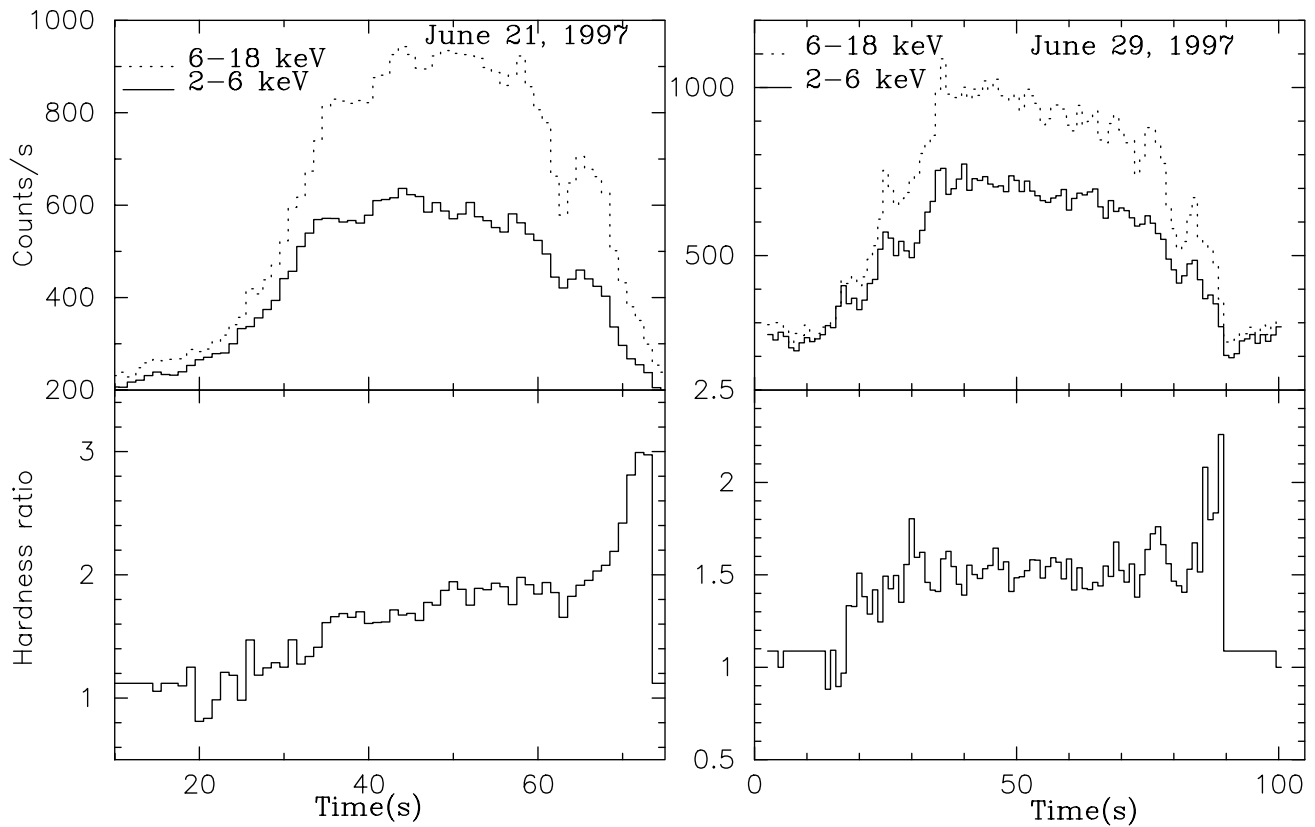
FIG. 3.—(a) Burst profiles in two different energy bands are shown in the top panels for the two types of regular bursts. The hardness ratio is shown in the bottom panels, and (b) the burst profiles in two different energy bands are shown in the top panels for the quasi-regular and irregular bursts. The hardness ratio is shown in the bottom panels.
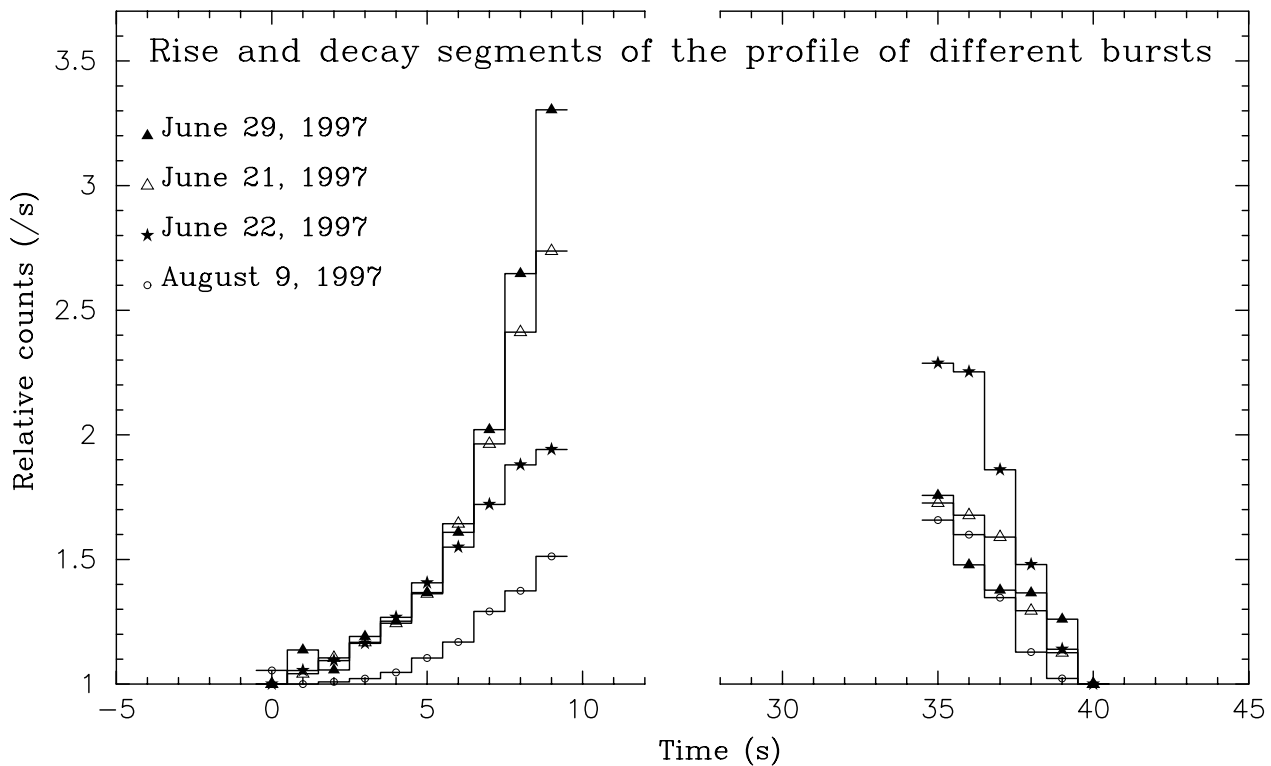
FIG. 4.—Rise and decay segments of the burst profile of all four types of observed bursts. The start time of the bursts is arbitrarily chosen at 0 s, and the end time at 40 s for clarity of comparison. The intensity of the rising segment is normalized to the start point while intensity of the decay segment is normalized to the end point.

sistent with a straight-line fit that gives a time constant (defined as the time required to drop from twice the quiescent flux) in the range of 3–7 s.

4. BURST STATISTICS

A summary of the characteristics of different type of bursts is given in Table 2. Also given in the table are mean quiescent and mean burst hardness ratio, defined as the ratio of counts in 6–18 keV to that in 2–6 keV. A total of 995 regular bursts of ~ 21 s recurrence time (in $\sim 20{,}700$ s of observation), 738 regular bursts of ~ 46 s recurrence time (in $\sim 33{,}560$ s of observation), 115 quasi-irregular bursts (in 6600 s) and 67 irregular bursts (in ~ 6890 s) have been detected. The peak intensity varies from 1.5 to 3.5 times the quiescent intensity.

In the case of quasi-regular and irregular bursts, the burst duration is correlated to the quiescent time just prior to the burst. We have measured the quiescent time and the burst duration for all types of bursts according to the definition given in the previous section. Results are shown in Figure 5 along with a least-squares straight-line fit that shows a good correlation between the burst duration and the preceding quiescent time for the quasi-regular and irregular bursts.

We do not see any such correlation for the regular bursts. Inclusion of the regular bursts reduces the correlation coefficient from 0.94 to 0.83 (shown in the inset of Fig. 5). Similar plots for the regular bursts of mean recurrence time 21 s and 46 s are shown in the top and bottom panels of Figure 6, respectively, for 3 days in each case. The dotted line is a least-square fit to the quasi-regular and irregular bursts and is shown here for comparison. For both the types of regular bursts, the burst duration is constant for each day, but it does show day-to-day variation. It may be stressed here that although the regular bursts themselves do not show any correlation between the preceding quiescent time and the burst duration, they fall very close to the relation derived for the quasi-regular and irregular bursts (see inset of Fig. 5). We do not find any correlation between the

TABLE 2

SUMMARY OF CHARACTERISTICS OF DIFFERENT TYPES OF BURSTS FROM GRS 1915+105

Type of Burst	Mean Recurrence Time or Interval (s)	Number of Bursts	Normalized Quiescent Flux[a]	Mean Quiescent HR[b]	Mean Burst HR[b]	Date of Observation
Regular	21 ± 3	995	2.87	1.28 ± 0.05	2.2 ± 0.2	Aug 7–10
Regular	46 ± 5	738	1.75	0.98 ± 0.02	1.2 ± 0.1	Jun 12–17 & Jun 22–26
Quasi-regular	50–90	115	1.2	0.94 ± 0.02	1.5 ± 0.1	Jun 19–21
Irregular	18–350	67	1.0	0.94 ± 0.02	1.5 ± 0.1	Jun 18 & June 27–29

[a] Quiescent flux is normalized to irregular bursts.
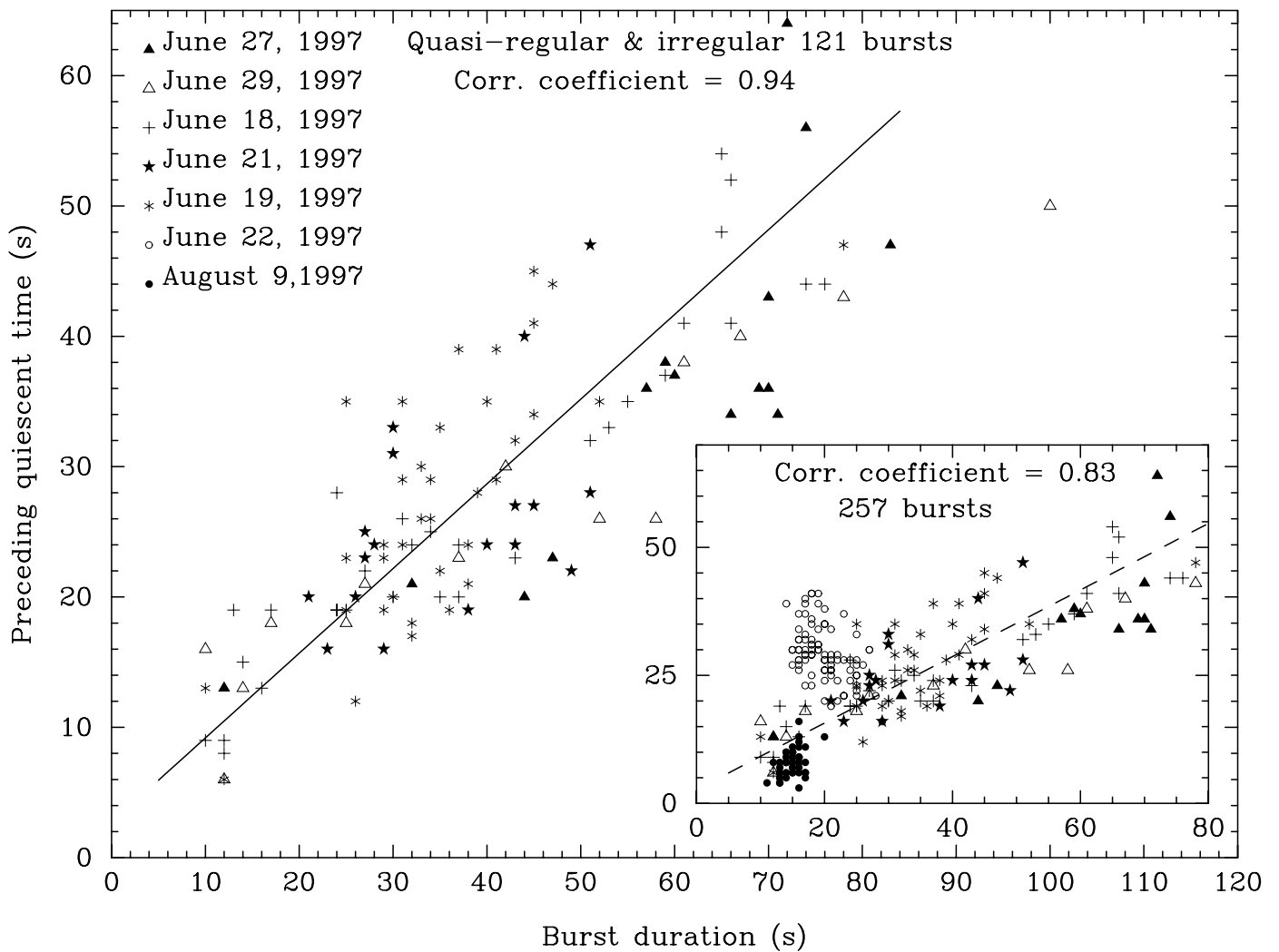[b] HR = hardness ratio and is defined as the ratio of counts in 6–18 keV to that in 2–6 keV bands.

FIG. 5.—Correlation between the preceding quiescent time and the burst duration (as defined in the text) for the quasi-regular and irregular bursts. The straight line is the least-squares fit to the data. In the inset, both types of regular bursts are also shown.

quiescent time following the burst and the burst duration and results for 257 different type of bursts are shown in Figure 7. The observed correlation for the burst duration and the preceding quiescent time for the irregular and quasi-regular bursts could be simply a reflection of the fact that the burst duration and the quiescent time are of comparable magnitude for such bursts. This correlation, however, establishes that a given burst cycle starts at the beginning of a quiescent phase and gets completed at the end of a burst phase because we do not find any correlation between the burst duration and the following quiescent time. Henceforth, we shall use the preceding quiescent time as the quiescent time of a burst. It is interesting to note that from 1997 June 17 to June 22 we observed continuously the full cycle of bursts, from regular to irregular to quasi-regular and again to regular.

We have calculated the average flux during the burst phase and during the quiescent phase separately for all the types of observed bursts, and results are shown in Figure 8. The ratio of average flux during the burst time to the average flux during the quiescent phase is plotted as a function of the burst duration. For quasi-regular and irregular bursts, this ratio shows good correlation with the burst duration (least-squares straight-line fit) and has a value of 2

and higher. This ratio is, however, constant and has a value of less than 2 for the regular bursts, as shown in the inset of Figure 8. The dotted line shows the least-squares straight-line fit for the quasi-regular and irregular bursts.

We have calculated average hardness ratio during the quiescent phase for all types of bursts and results are shown in Figure 9. The hardness ratio decreases as the quiescent time increases, and it is higher for the regular bursts than that for the quasi-regular and irregular bursts. The ratio of average flux during the burst time to the average flux during the quiescent phase is plotted in Figure 10 as a function of the average hardness ratio during the quiescent phase for all the observed bursts. The solid line is a least-squares fit to both types of regular burst data (442 regular bursts), which shows good correlation.

5. DISCUSSION

Because of their unique feature of slow rise and fast decay, the bursts in GRS 1915+105 are very different from the type I X-ray bursts seen in about 40 LMXBs and type II X-ray bursts in the Rapid Burster (MXB 1730-335). All the bursts in the LMXBs have fast rise time of less than a second to a few seconds and slow decay of 10 s to a few minutes (Lewin et al. 1995). The type I X-ray bursts are
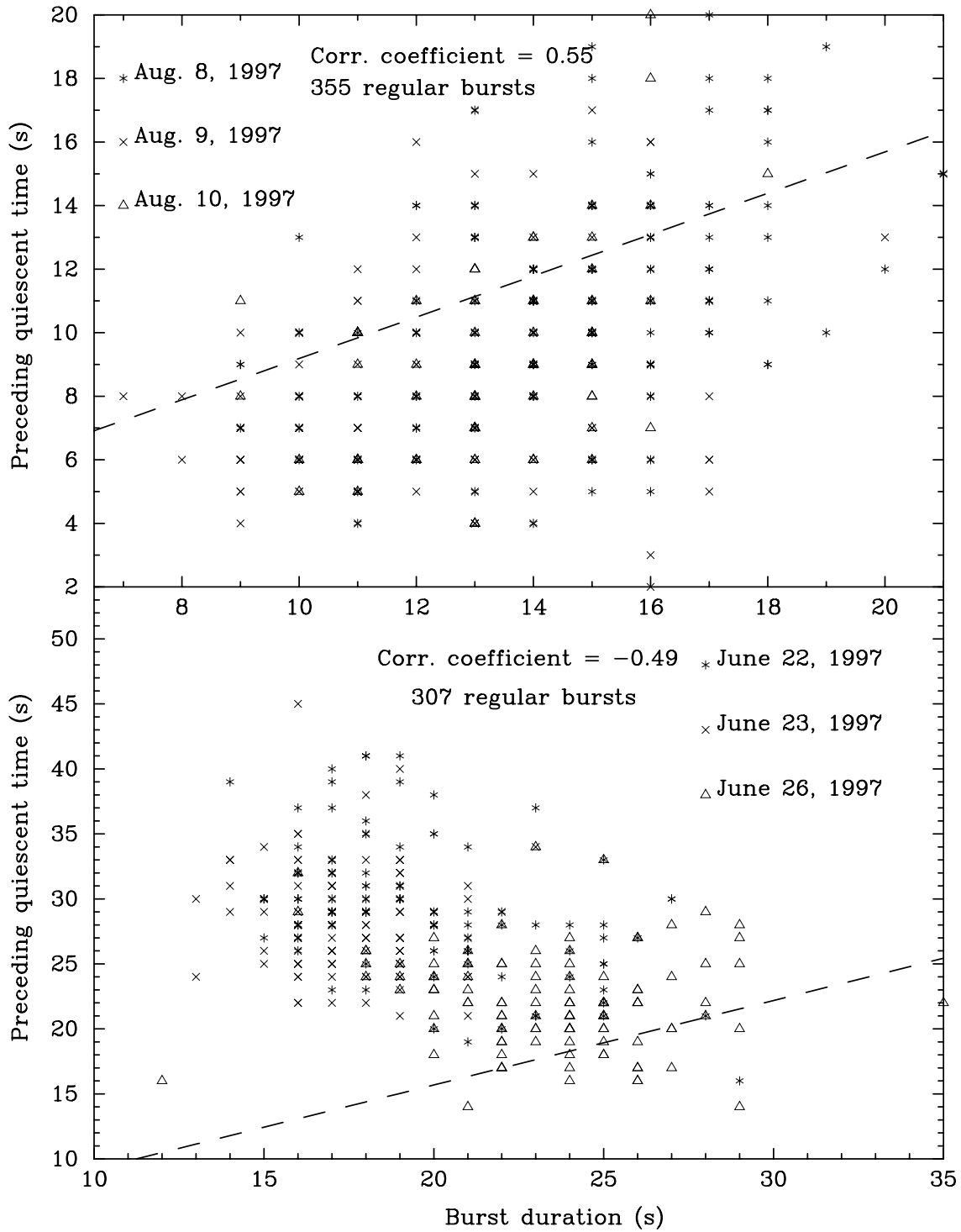
FIG. 6.—Correlation between the preceding quiescent time and the burst duration for the regular bursts with ~21 s recurrence time in the top panel and for the regular bursts with ~46 s recurrence time in the bottom panel. Data are for 3 days in each case. The least-squares fit for the quasi-regular and irregular bursts (of Fig. 5) is shown by dotted line for comparison.

understood to be thermonuclear flashes caused by accretion of matter onto the surface of the neutron star. The type II bursts are produced by sudden infall of matter on to the neutron star owing to some instability in the inner part of the accretion disk supported by the magnetic field. The slow decay of the burst intensity represents the cooling timescale of the neutron star photosphere. In the classical bursts, the spectrum is initially hard and becomes softer as the burst

decays (Lewin et al. 1995). In sharp contrast, the bursts in GRS 1915+105 remain hard till the end and are, in fact, hardest near the end of the burst.

In the case of type I X-ray bursts, the ratio of the burst luminosity (L_b) and the average quiescent X-ray luminosity (L_p) is $L_b/L_p \sim 10^{-2}$. On the other hand, the time-averaged type II burst luminosity is much higher, usually 0.4 to 2.2 times the average luminosity of quiescent emission (Lewin
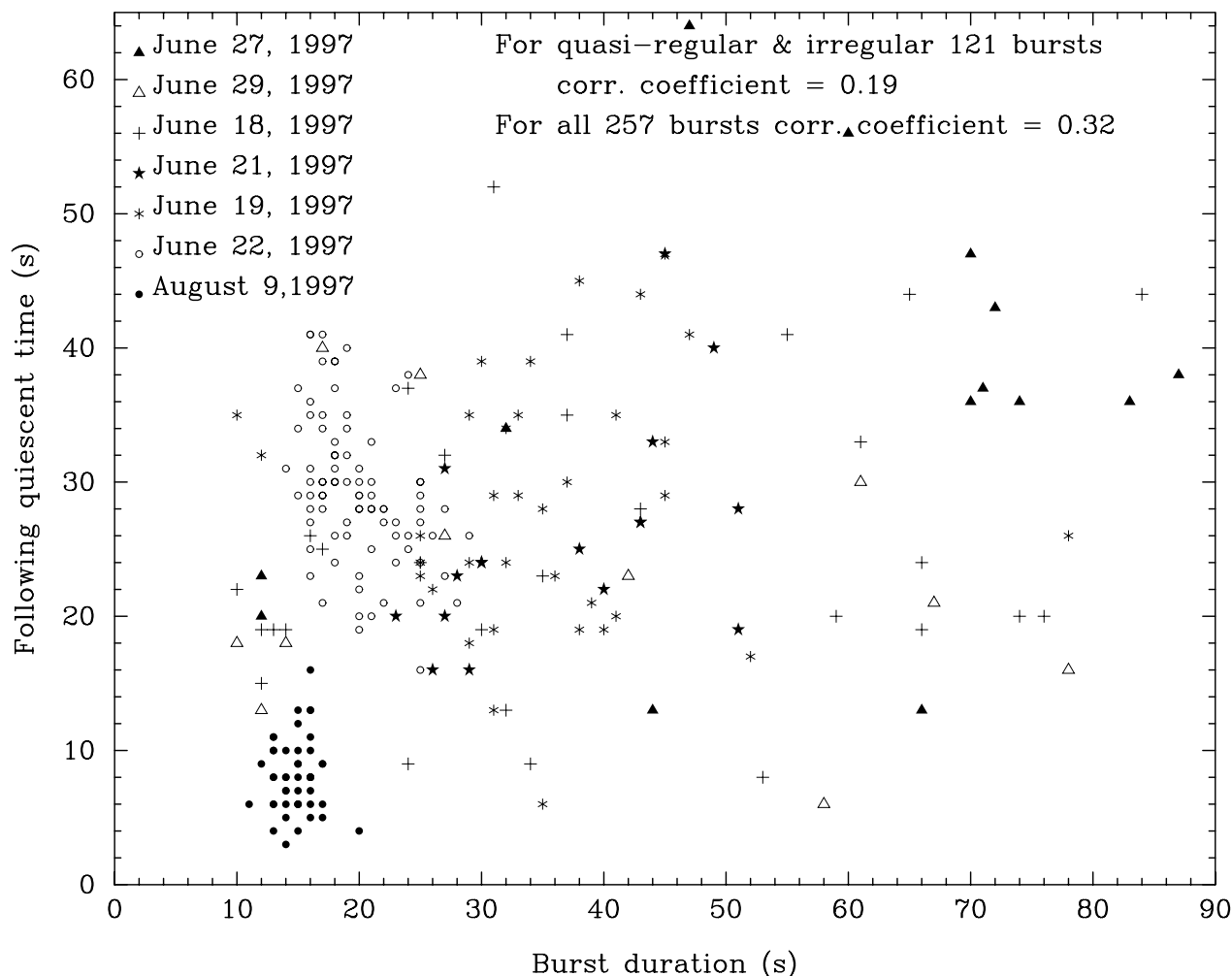
Fig. 7.—Correlation between following quiescent time and the burst duration (as defined in the text) for the same data as in Fig. 5

et al. 1995). The time-averaged luminosity of the regular bursts detected from GRS 1915+105 is 0.15–0.9 times the luminosity of the quiescent emission. This is much higher than the ratio in type I bursts (where the thermonuclear process has much smaller efficiency compared to the gravitational process) and less than the type II bursts (where the burst emission is due to gravitational energy release). The emission process involved in producing the bursts here is not likely to be thermonuclear because of the energetics involved. If the energy generation process is gravitational (like in type II bursts), the difference in efficiency might indicate the absence of hard surface in the compact object. A process in which the energy produced is due to gravitational potential but not all the energy is emitted as radiation, part of it being advected into the event horizon as kinetic energy of the matter, is appropriate for this source. This probably provides compelling evidence that the compact object in GRS 1915+105 may be a black hole.

The quasi-regular and irregular bursts show higher variability near the end of the burst as we noted earlier and the burst duration is correlated to the quiescent time. Similar behavior is also reported from the PCA observations carried out in 1996 June (Belloni et al. 1997a). Several irregular bursts, concurrent with the present observations on 1997 June 18 and having similar properties, have also been detected in the PCA data (Belloni et al. 1997b). They

modeled these bursts as a consequence of emptying and replenishing of the inner accretion disk caused by a viscous thermal instability. Paul et al. (1998b), on the other hand, attempted to explain the regular bursts as due to periodic infall of matter onto a black hole from an oscillating shock front. In the following we attempt to give a comprehensive picture of the various types of burst observed in GRS 1915+105 in the light of the recent theories of advective accretion disks.

5.1. Advective Accretion Flows around Black Holes

Recent work on the theory of accretion onto black holes (see Abramowicz & Percival 1997; Chakrabarti 1996b; Narayan et al. 1998 for reviews) has shown that advection cooling is important in the innermost part of the accretion disk. For hot optically thin disks strong advective cooling occurs everywhere, very far from the black hole as well.

Narayan & Yi (1994) have taken a self-similar solution and have divided the possible solutions into two branches: the first type where the energy is trapped from the disk and converted to jets and the second type with advection dominated thick accretion disk. A few observed sources are compared with the predictions of the advective-dominated accretion flows (ADAF) with a fair degree of success (Narayan et al. 1997b). Chakrabarti & Titarchuk (1995), on the other hand, have taken a complete solution of viscous
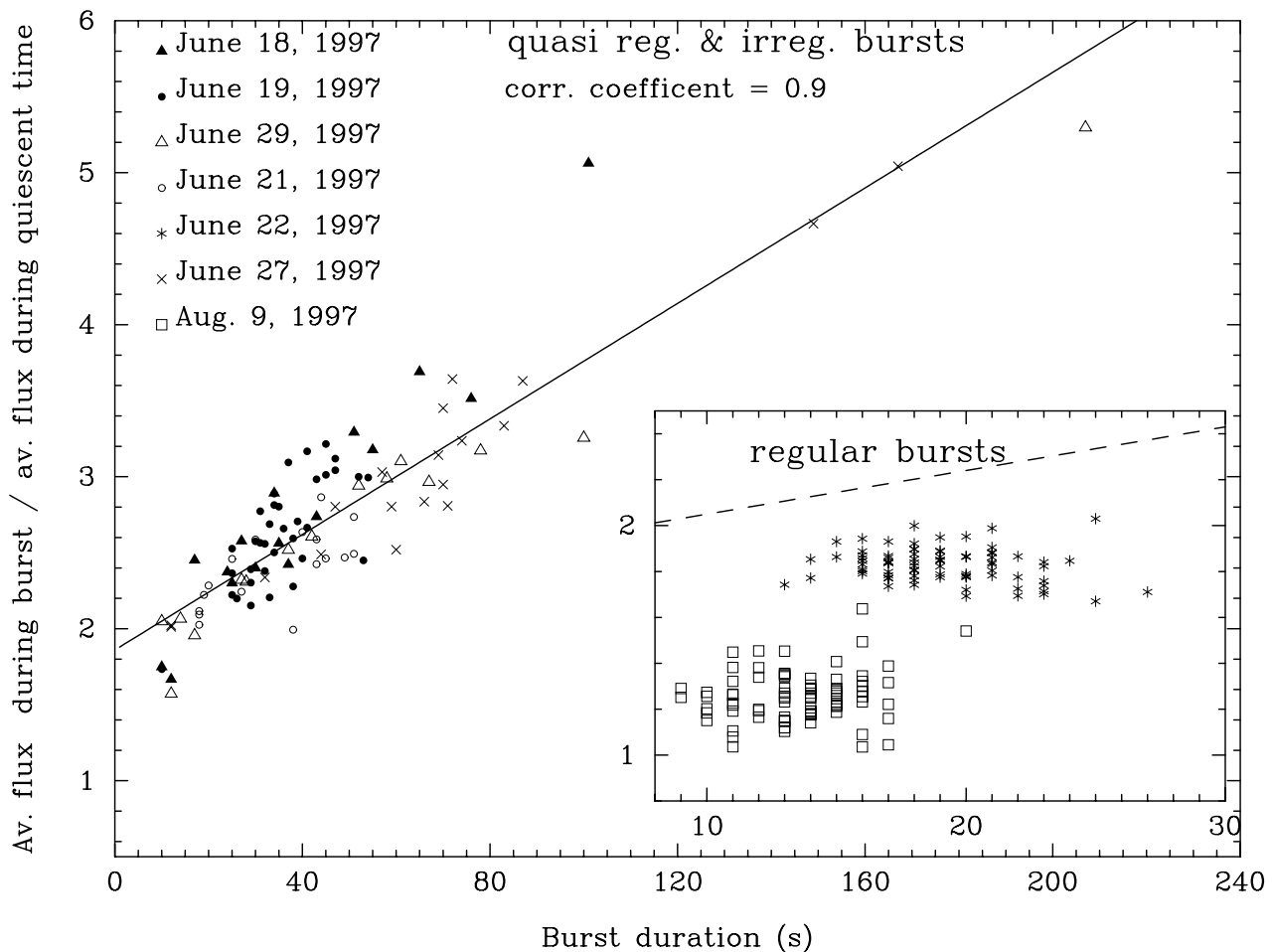
FIG. 8.—Ratio of the average flux during burst to the average flux during quiescent time as a function of the burst duration for the quasi-regular and irregular bursts. The solid line is the least-squares fit to the data. In the inset, results for both types of regular bursts are shown. The dotted line is the fit for the quasi-regular and irregular bursts and is shown for comparison.

transonic equations and demonstrated that the accretion disk has a highly viscous Keplerian part that resides on the equatorial plane and a sub-Keplerian component that resides above and below it. The sub-Keplerian component can form a standing shock wave (or, more generally, a centrifugal barrier-supported dense region) that heats up the disk to a high temperature. The need to define the viscosity parameter is circumvented by taking two accretion rates: accretion through the classical "standard" disk and accretion through the sub-Keplerian component. Ebisawa, Titarchuk, & Chakrabarti (1996) have attempted to explain the observed X-ray spectrum, particularly the change of spectral states in the black hole candidates, using this model. In both models the changes of spectral states are ascribed to the changeover from a purely thin accretion disk (with advection occurring very close to the black hole) in the high-soft state to the advective disk extending over a large distance in the low-hard state. The hard X-ray power-law component is ascribed to the Comptonization spectrum from the advective disk and the Shakura-Sunyaev multi-temperature disk emission (which is predominant in energies below ~ 10 keV) is associated with the standard thin disk. In the ADAF model of Narayan & Yi (1994), the advective thick disk changes into a standard thin disk at a distance r_{tr}, whereas, according to Chakrabarti & Titarchuk (1995), the advective thick disk and the standard thin

disk coexist up to a certain radial distance and a standing shock wave or a centrifugal barrier-dominated dense region is a common feature of the sub-Keplerian component. In the following we try to examine the burst properties of GRS 1915+105 in the light of these new accretion disk theories that incorporate advection.

The source was in a low-hard state from 1996 December to 1997 March (Greiner et al. 1998), when the hard X-ray spectral index (~ 2.0) and the soft X-ray flux (300–500 mcrab) were low. The source started a new outburst around 1997 April–May, when the soft X-ray flux started increasing and the X-ray spectrum became soft (spectral index increased to 3–4). We suggest that the peculiar bursts that we have seen are characteristics of the change of state of the source.

In the quiescent state of the burst the source is in the hard state. This is evident from the large value derived for the inner disk radius (R_{in}) of the multitemperature thin-disk model fitted for the energy spectrum. The fitted value of R_{in} is around 300 km for very long bursts of 1000 s duration (Belloni et al. 1997a), 30–100 km for the irregular bursts (Belloni et al. 1997b), and 30 km for regular bursts (Taam et al. 1997). Note that the derived values for the radius can be underestimated because of scattering effects and because of the approximation involved in fitting the Comptonized part of the spectrum as a power law (see Shrader & Titarchuk
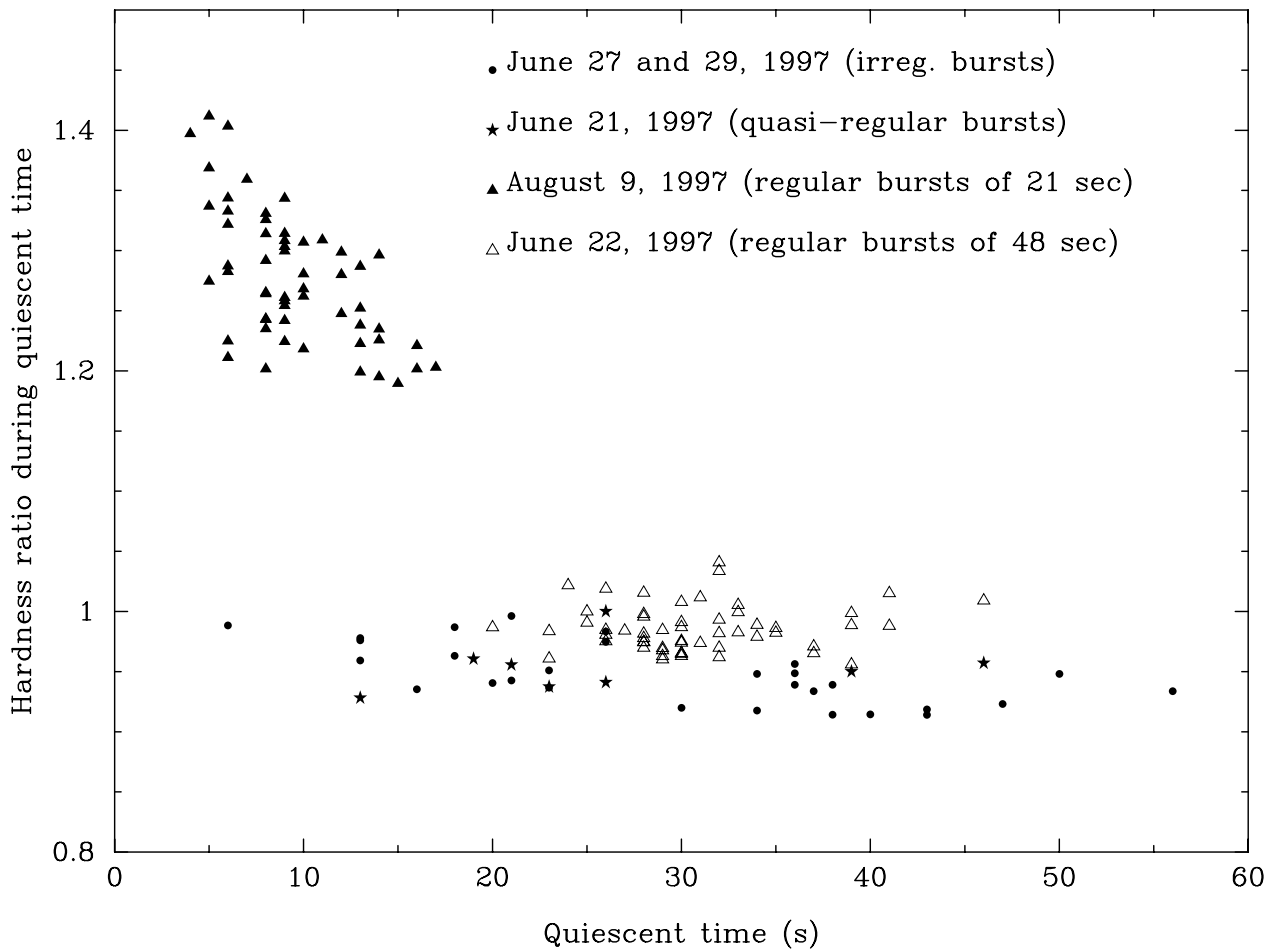
FIG. 9.—Hardness ratio during the quiescent phase vs. the quiescent time for all type of observed bursts from GRS 1915+105

1998). It should be further noted that the derivation of R_{in} is very much model dependent and we use this quantity only for a qualitative description of the spectral states and to make an order-of-magnitude estimate of timescales involved in the change of spectral states. The fitted temperature of the disk is 1–1.5 keV. The spectral index of the power-law component during the quiescent state of the long bursts is ~ 2.22 (Belloni et al. 1997a), indicating that the source is truly in a hard state. During the burst phase the intensity is higher, the radius of the disk is smaller (20–30 km), the temperature is higher (2–3 keV), and the power-law index is steeper (3.57 for the long bursts and 3.3 for the regular bursts). These characteristics strongly suggest that the source is in a high-soft state during the bursts. Hence there are strong indications that the source makes state transitions in very short timescales corresponding to the rise and fall time of the bursts (a few seconds). Such fast changes of states are possible in the two-component accretion flows where the advective disk covers the standard thin disk (Chakrabarti 1996b). In the following we describe the bursting behaviors of GRS 1915+105 within this scenario, taking the model parameters given in Chakrabarti & Titarchuk (1995) and also in Narayan et al. (1998).

In the low-hard state of the source the thin Keplerian disk is visible only from a large radial distance R_o, the sub-Keplerian component completely encompasses the thin disk below this radius (the soft photons from the disk act as seeds for the Comptonization process). When the disk acc-

retion rate $(\dot{m}_d)$ increases, at some critical point the non-Keplerian halo accretion rate $(\dot{m}_h)$ can decrease and the high-soft state can set in. This change in accretion rate can occur either because of the change in the total accretion rate $(\dot{m}_t = \dot{m}_d + \dot{m}_h)$ or because of some change in the viscosity in the thin accretion disk that changes $\dot{m}_d$ (keeping $\dot{m}_t$ constant). We suggest that when the total accretion rate is close to some critical value, the source can change states and the observed irregular bursts are the manifestations of such changes of state.

To understand the mechanism of the bursts let us equate R_{in} to R_o, from where the advection dominated halo component starts covering the thin accretion disk in the low-hard state of the source (the quiescent state of the burst). Assume that $\dot{m}_d$ is close to a critical value where the change of the state takes place. At some particular point of time the boundary condition at the inner edge changes such that $\dot{m}_d$ increases. The spectral state, however, will remain unchanged till this effect reaches R_o. The timescale for this to happen is the viscous timescale of the thin accretion disk. Assuming the standard α disc, we can write the viscous timescale as R_o^2/ν, where ν is the viscosity coefficient that is given as $\alpha c_s H$ for the α disk, where c_s is the sound speed, H is the disk thickness, and α is the viscosity parameter. Taking the scaling laws for H and c_s (Frank, King, & Raine 1985), we can write the viscous timescale of the disk as

$$t_{vis}^d = 4.3 \times 10^{-4} \alpha^{-1} \dot{m}_d^{-1} m^{-1} R_o^2 \text{ s}, \qquad (1)$$
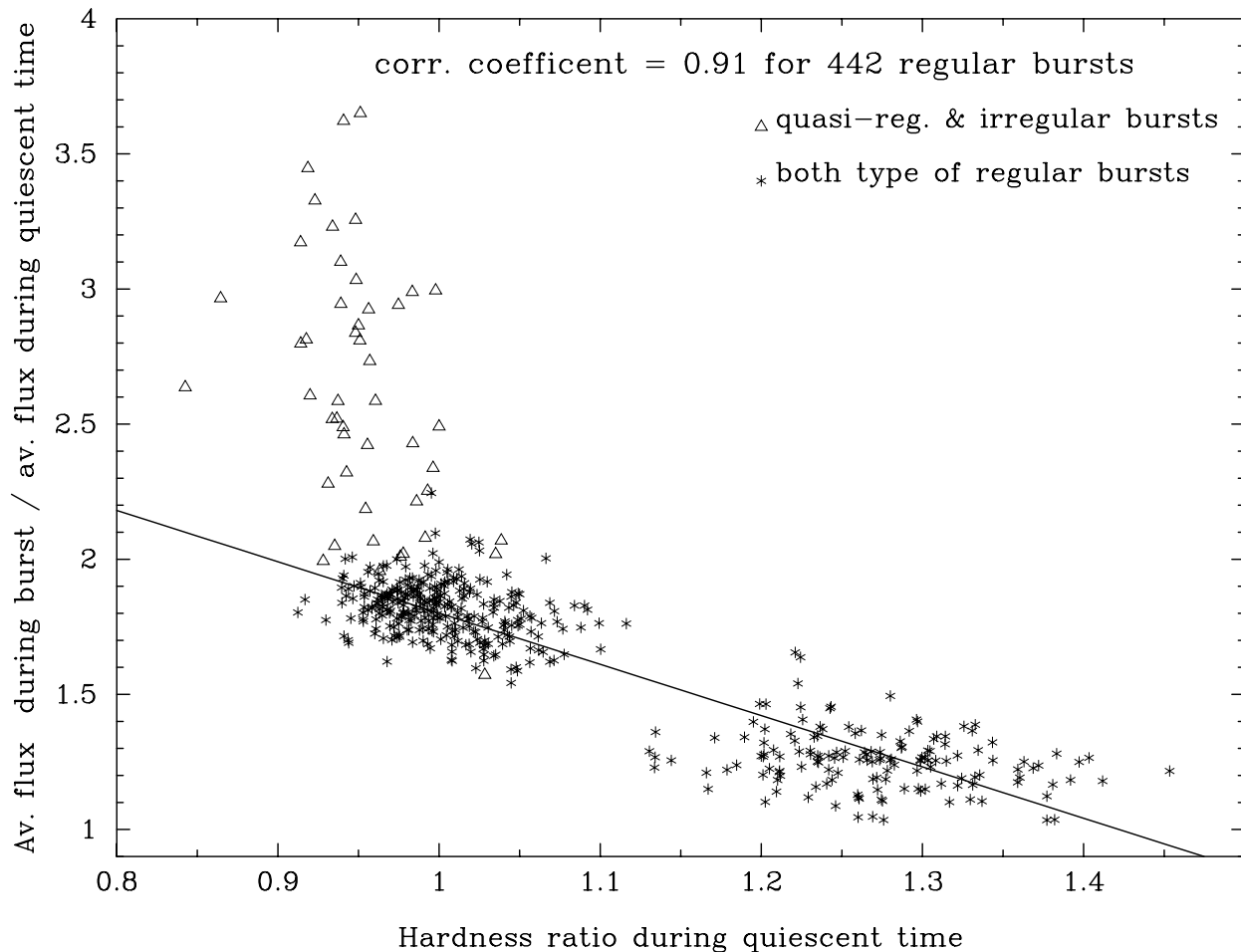
FIG. 10.—Ratio of the average flux during burst to the average flux during the quiescent time as a function of the hardness ratio during the quiescent time for all the type of observed bursts. The least-squares fit to both types of regular burst is shown by a solid line.

where $\dot{m}_d$ is in the units of Eddington accretion rate and m is the mass of the black hole in solar mass units and R_o is in km. Substituting $\dot{m}_d = 1$, $m = 0$, $\alpha = 0.01$, and $R_o = 300$, we get $t_{\rm vis} = 400$ s, agreeing with the observed quiescent state timescale of long bursts. This also explains the nonlinear dependence of burst quiescent time on radius, reported by Belloni et al. (1997b) for the long irregular bursts.

At R_o, the increased $\dot{m}_d$ decreases $\dot{m}_h$ and the advection dominated halo component completely advects onto the black hole in the viscous timescale of the halo component given by

$$t_{\rm vis}^h = \frac{R_o^2}{H \alpha c_s} .$$ (2)

Here we assume that the halo component is an advection-dominated accretion disk in which the temperature can go very high (see Narayan et al. 1998). For advection-dominated thick disks we can take $H \sim R$ and use the scaling law for c_s as

$$c_s = 1.18 \times 10^{10} (R_o/R_s)^{-1/2} \ {\rm cm}^{-1} ,$$ (3)

where R_s is the Schwarzschild radius (Narayan et al. 1998). We can rewrite the viscous timescale as

$$t_{\rm vis}^h = 4.9 \times 10^{-6} \alpha^{-1} m^{-1/2} R_o^{3/2} \ {\rm s} .$$ (4)

Substituting the values as earlier, we get $t_{\rm vis}^h$ as ~ 1 s, which is quite close to the observed rise time of the burst. Now the burst phase starts, which is nothing but the soft state of the source with R_o coming very close to the shock front (or the centrifugal barrier supported dense region). Note that the value of R_o derived by spectral fitting is always 20–30 km during the burst maximum, irrespective of the type of the burst. At some particular time the inner boundary condition can change again, $\dot{m}_d$ can decrease and $\dot{m}_h$ can increase, and this sub-Keplerian component can suppress inner part of the accretion disk and a Compton cloud can be generated. In the advection-dominated accretion flow, the radial velocity, typically, will be

$$v = -1.9 \times 10^{10} \alpha R_o^{-1/2} m^{-1/2} \ {\rm cm \ s}^{-1}$$ (5)

(see Narayan et al. 1998). For a radius of 300 km, this will have a timescale of ~ 1 s, which is seen as the fast decay time of the bursts.

For smaller values of R_o, the infall timescale will be lower (it goes as $R_o^{3/2}$), and for some particular value of R_o this timescale can match the cooling timescale of the postshock region, which is about 0.01 s for a shock radius $20 r_g$ (where r_g is the Schwarzschild radius) and black hole mass of 10 $M_\odot$ (Paul et al. 1998b). When the two timescales match they can give rise to oscillations that are quasi-periodic in nature (Molteni, Sponholz, & Chakrabarti 1996). The infalling matter can immediately trigger the instability at the inner

boundary of the disk and the source can immediately revert back to the hard state.

These regular oscillations accumulate matter at the shock front (or the centrifugal barrier) and they can catastrophically fall onto the black hole. The scenario described above explains in a qualitative way the various types of bursts observed in GRS 1915+105. We must mention here that the timescales and sizes that we have taken for the calculations are very approximate because of the uncertainties in the multitemperature disk parameters and the viscosity parameter.

The scenario sketched above is similar to that described by Belloni et al. (1997a) as far as the viscous timescale is concerned. These authors, however, make the assumption that when the source reverts back to the low-intensity state of the burst, the matter between R_o and R_{in} disappears behind the black hole at a free fall timescale. It is worth pointing out that a standard thin accretion disk cannot disappear at free-fall timescale without effectively transferring its angular momentum and the timescale for angular momentum transfer is the viscous timescale. Further, the systematic change in the hard power-law index during the bursts cannot be explained only by invoking a change in the disk inner radius.

Paul et al. (1998b) have explained the regular bursts in terms of the oscillations of the shock front. For this to happen in the observed timescale, the shock has to be very far away from the black hole. This can happen only in the low state of the source. Actual observations, however, suggest that the regular bursts occur when the source approaches the soft-high state when the shock front is very close to the compact object. Hence it appears that the periodicity of the regular bursts occurs from the matching of the viscous timescales rather than the shock front oscillation. The catastrophic infall of matter at the shock front, invoked by Paul et al. (1998b), seems to be appropriate for the regular bursts.

Several of the correlations obtained in the preceding sections can be explained using the physical picture described above. The quiescent flux is related to R_o (see Table 2). The rise time of the bursts represents the viscous timescales of the halo component. The burst duration is related to the preceding quiescent time (Fig. 5) because the timescale for the inner boundary condition to change will also be the viscous timescale, which is related to the R_o of the preceding quiescent time. This correlation does not hold for the regular bursts because the burst duration is independent of R_o owing to the resonance. During quasi-regular and irregular bursts, change in $\dot{m}_d$ is mainly due to change in viscosity caused by a viscous thermal instability (see Fig. 9; the variation in hardness ratio for these bursts during quiescent time is much less than that in case of regular bursts) (Belloni et al. 1997a). The high quiescent time X-ray flux during the regular bursts heats up the disk and suppresses the instability (Lewin et al. 1995).

The ratio of the average fluxes during the burst and the quiescent time essentially represents the ratio of the values for R_o, which is related to the burst duration through the relation for the viscous timescale (Fig. 8). The hardness ratio (which represents the inner disk temperature) shows weak dependence on the quiescent time for the irregular bursts because for large enough R_o the temperature does not change drastically with R_o (Fig. 9). The regular bursts of long duration (45 s) also have a value for the hardness ratio

during quiescent time, which is similar to that seen for the irregular bursts (though slightly higher). The variation in hardness ratio is larger, which reflects the change in R_o (see Fig. 10). The mean burst hardness ratio for these bursts is ~ 1.2, which suggests that these bursts occur during high state (Narayan et al. 1998). During the short duration regular bursts the source is almost in the soft-high state during the quiescent phase, showing a large value for the hardness ratio. The mean burst hardness ratio is ~ 2.2, which suggests very high state. These observations imply that $\dot{m}_d$ is substantially larger in very high state than that in high state. The flux ratio for the regular bursts represents the amount of amplification that is possible for the resonating bursts, and it is related to the quiescent time temperature (Fig. 10).

According to the scenario sketched above, the X-ray bursts are due to fast changes in the spectral states when the source reaches the high state and the accretion rate is very close to the Eddington accretion rate. Chakrabarti & Titarchuk (1995) have pointed out that during such a high state the source shows a distinct hard spectral component due to bulk motion Comptonization. Shrader & Titarchuk (1998) have fitted the high-state spectrum of GRS 1915+105 using the bulk motion Comptonization model and derived a temperature of 0.9 keV. Titarchuk & Zannias (1998) have analyzed the exact general relativistic integrodifferential equation of radiative transfer for a realistic situation of accretion onto black holes in the high state and showed that an extended power-law spectrum results even from an arbitrary spectrum of low-energy photons. Laurent & Titarchuk (1999) have calculated the specific features of X-ray spectra using Monte Carlo simulations and demonstrated the stability of power-law spectral index over a wide range of mass accretion rates. This conclusion agrees with our observation that the hardness ratio during the quiescent time remains constant over wide burst timescales (Fig. 9), except for the regular bursts of 21 s duration, which may be due to reduced optical depth (thus the halo) for these bursts.

It is interesting to speculate about the possible reasons for the differences in the two regular bursts of ~ 21 s and ~ 46 s duration. As pointed out by Shrader & Titarchuk (1998), bulk motion Comptonization sets in during the soft-high state and the energy radiated is a very small fraction of the accretion energy. Part of the energy can be used to drive the matter away from the central source in terms of jets. The difference in the two regular bursts may be due to the fact that in the regular bursts of 21 s duration jet formation may be setting in. It may be noted here that the time profiles of the two types of regular bursts agree with each other but for a sharp dip in the short regular bursts.

The ADAF models have been used to obtain unique identifying features of black hole sources (Narayan et al. 1997a; Laurent & Titarchuk 1999). An advection-dominated accretion flow is one in which most of the energy released by viscous dissipation is stored in the gas and advected to the compact object and a small fraction of the energy is radiated. The argument is that if accretion is via an ADAF and if the object has an event horizon, then the advection energy will disappear from sight. However, if the central object has a surface, then the surface will be heated by the hot inflow from the ADAF and the advected energy will be emitted as thermal radiation. This additional evidence for the black hole nature of GRS 1915+105 is qualitatively different from usual method that rely on a

measurement of the mass. The usual argument is that if an object is too massive to be a neutron star, it must be a black hole.

5.2. *A Test of the Model using* RXTE/*PCA Data*

In principle, one can test this model using X-ray data above 10 keV. The Shakura-Sunyaev multitemperature disk emission dominates in $2-10$ keV energy range, while the power-law component dominates at higher energies (Shrader & Titarchuk 1998). We have analyzed the publicly available *RXTE*/PCA data for irregular as well as regular bursts concurrent with our observations. The results of irregular bursts from *RXTE*/PCA data of 1997 June 18 are shown in Figure 11 along with the results from *RXTE*/PCA data of 1997 May 8 and August 19, when GRS 1915+105 was in low state and in high state, respectively. Both the top and the bottom panels have same y-axis scales. Similarly, both the left panels and the right panels (*top and bottom*) have same x-axis scales. This allows straightforward comparison of burst time data with the data during low and high state. GRS 1915+105 was in high state on 1997 August 19 and 2-13 keV flux varied from 19,000 counts s^{-1} to 30,000 counts s^{-1}, while the source was in low state on 1997 May 8 and $2-13$ keV flux was steady around 6000 counts s^{-1} (*right top panel*). No burst is observed during

these observations. The ratio of 13–60 keV flux to 2–13 keV flux has a value of 12% ± 2% during the low state on 1997 May 8, while it is ∼3% during the high state on 1997 August 19 (*bottom right panel*). This implies that the source remains in the same state during these observations.

The results of irregular bursts on 1997 June 18 are shown in left panels of Figure 11. The 2–13 keV flux varies from 4000 counts s^{-1} to 28,000 counts s^{-1}, which is shown in left top panel. These bursts have similar profile as those shown in second panel (*from top*) of Figure 1 from our data of 2–18 keV for June 27. The ratio of 13–60 keV flux to 2–13 keV flux is shown in left bottom panel. The relative flux of 13–60 keV reaches up to 12% during quiescent time, while it is as low as 3% during burst phase of irregular bursts. The minimum value of this ratio during burst phase is in agreement with the value of this ratio for the high state on 1997 August 19. Similarly, its maximum value during quiescent phase is in agreement with the value for low state on 1997 May 8. The 13–60/2–13 ratio drops to its minimum value of ∼3% at the first peak of each burst, which implies cooling of the halo component by the soft photons from the disk. It starts increasing immediately during the rest of the burst phase. This ratio reaches a value of ∼6% during the burst decay phase, which would mean a significant recovery of the halo component. The burst decay phase, therefore, may rep-
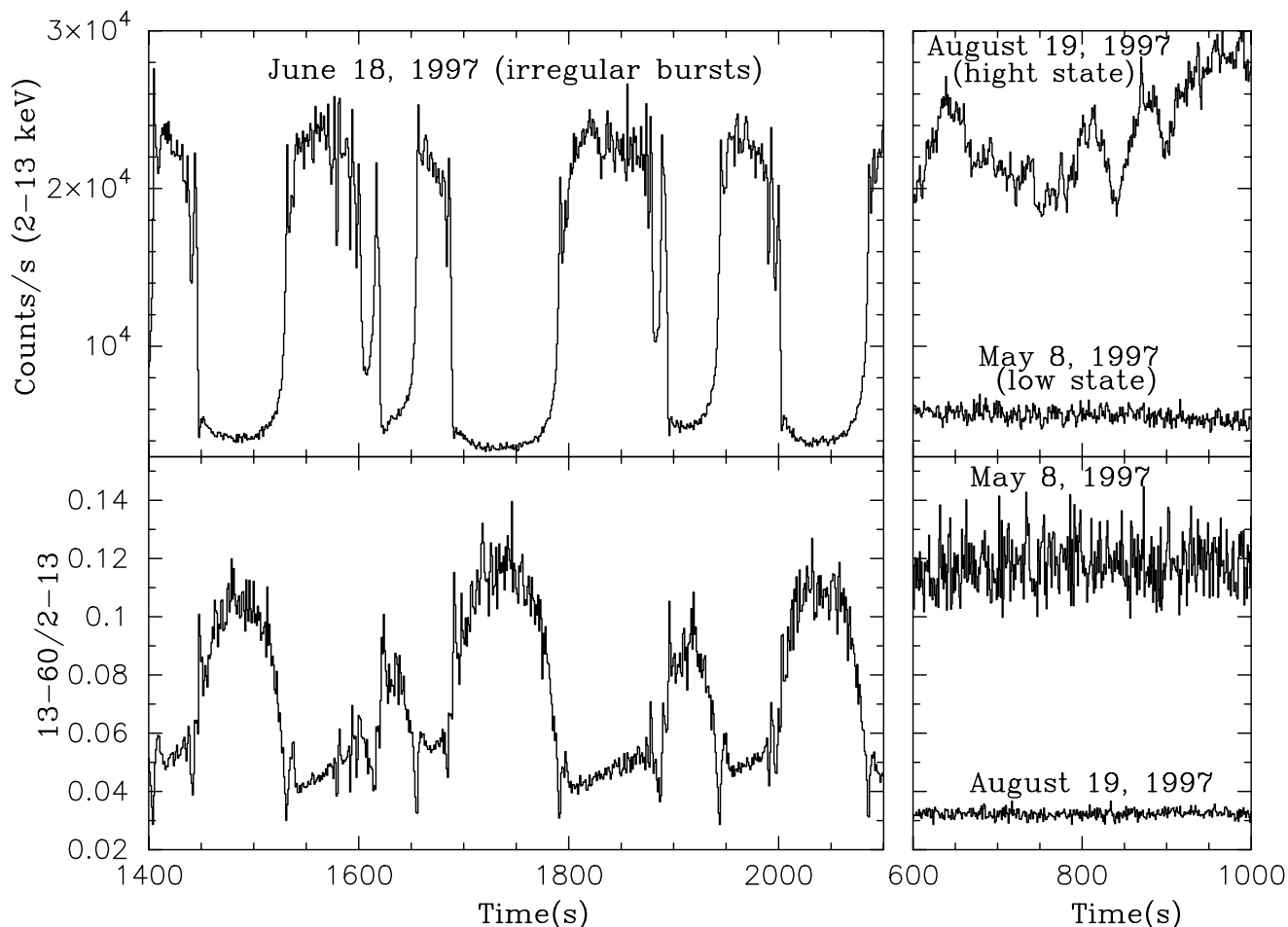

FIG. 11.—Plot of 2–13 keV flux vs. time is shown in left top panel (irregular bursts) and the ratio of 13–60 keV flux to 2–13 keV flux is plotted as a function of time in the left bottom panel from *RXTE*/PCA data of 1997 June 18. In the right top panel, 2–13 keV flux is plotted from *RXTE*/PCA data of 1997 August 19 and May 8, when source was in high and low states, respectively. Respective ratios of 13–60 keV flux to 2–13 keV flux are plotted in the right bottom panel.

resent unsaturated Comptonization before the source reaches saturated level of low state.

Similar results of regular bursts from *RXTE*/PCA data of 1997 June 22 are shown in Figure 12. The 2–13 keV flux varies from 7000 counts s^{-1} to 29,000 counts s^{-1} (*top panel*). The ratio of 13–60 keV flux to 2–13 keV flux reaches up to 9% during quiescent time, and it drops up to ∼3.5 % during burst phase of regular bursts (*bottom panel*). One would expect the contribution from the power-law component to be higher in the case of irregular bursts than that for regular bursts because of larger R_o. This would mean that resonance terminates the recovery of the halo component prematurely in the case of regular bursts. In fact, this is the major difference between the regular bursts and the irregular bursts, as much longer time is available for the recovery of the halo component in the case of irregular bursts. During burst phases, the relative contribution of the power-law component is lower in case of regular bursts, as the thin accretion disk extends to a smaller radius and hence has a temperature higher than those of irregular bursts (see Fig. 10) The results of the other type of regular bursts of ∼21 s duration are also consistent with this scenario. The ratio of 13–60 keV flux to 2–13 keV flux reaches up to 6% during quiescent time. The 2–13 keV maximum flux during burst phase is the same (approaching a value of 28,000 counts s^{-1} for five CPUs of *RXTE*/PCA) for all the types of observed bursts, providing another independent support to our model, while the quiescent time minimum flux varies almost by a factor of 4.

6. CONCLUSION

The observed bursts from GRS 1915+105 are very different than the classical bursts in LMXBs both in terms of temporal structure and spectral evolution. Our results broadly put all the observed bursts in two classes: irregular and quasi-regular bursts in one class, and regular bursts in another. There is a strong correlation between the preceding quiescent time and the burst duration for the quasi-regular and irregular bursts. No such correlation is found for the regular bursts. The ratio of average flux during the burst time to the average flux during the quiescent phase is high and variable in former case while it is low and constant in latter case. We present a comprehensive picture of the various types of bursts observed in GRS 1915+105 in the light of the recent theories of advective accretion disks. We present a unified model for the origin of these bursts that explains almost all the observed properties of these bursts. We suggest that the peculiar bursts that we have seen are characteristic of the change of state of the source. The change of state is due to change in the disk accretion rate, which may be due either to a change in the total accretion rate or to changes in the viscosity in the thin accretion disk. The periodicity of the regular bursts occurs from matching of the viscous timescale with the cooling timescale of the postshock region. We have presented a test of this model, using 13–60 keV *RXTE*/PCA data for irregular bursts and regular bursts during the low-hard state and during the high-soft state, which show good agreement with our
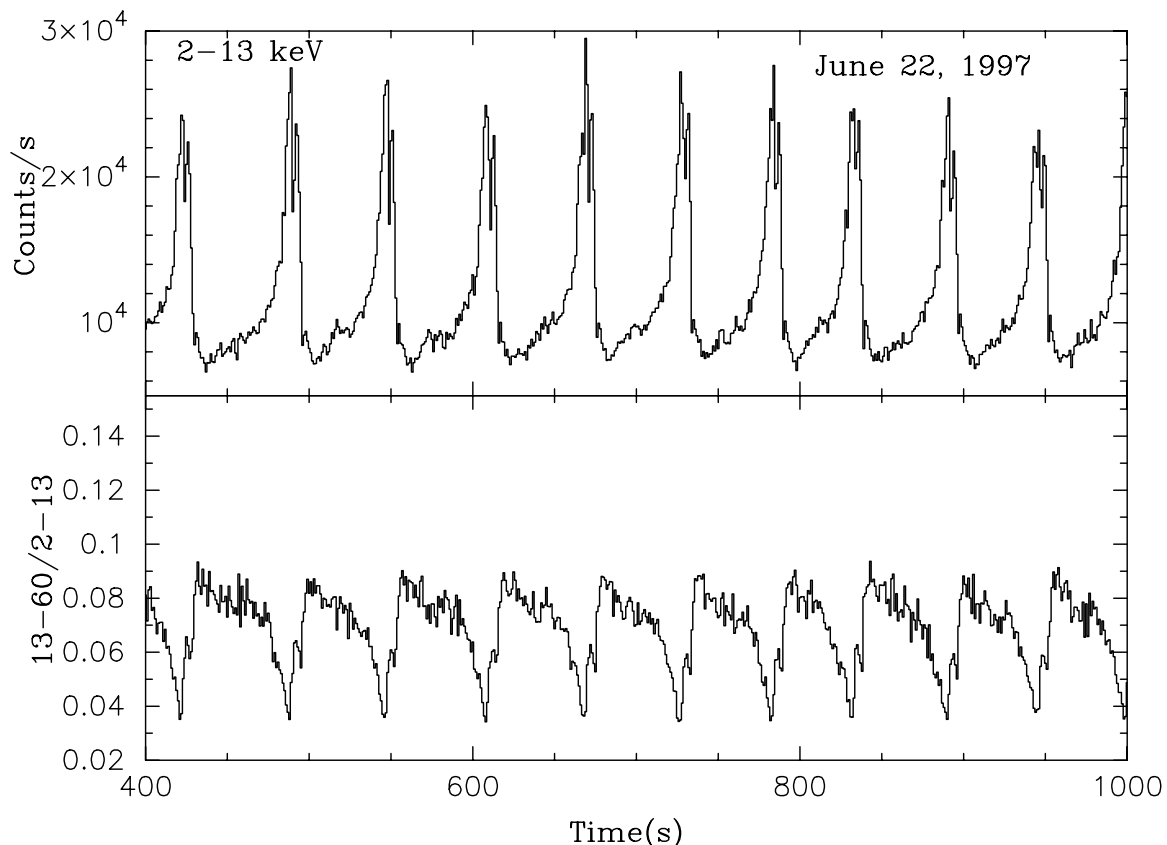

Fig. 12.—Plot of 2–13 keV flux vs. time is shown in the top panel (*regular bursts*) and the ratio of 13–60 keV flux to 2–13 keV flux is plotted as a function of time in the bottom panel from *RXTE*/PCA data of 1997 June 22.

model. These results may be viewed as additional evidence that the X-ray source GRS 1915 + 105 is a black hole.

REFERENCES

Abramowicz, M. A., & Percival, M. J. 1997, Classical Quantum Gravity, 14, 2003
Agrawal, P. C., et al. 1996, IAU Circ. 6488
————. 1997, J. Korean Astron. Soc., 29, S429
Belloni, T., et al. 1997a, ApJ, 479, L145
————. 1997b, ApJ, 488, L109
Bradt, H. 1996, preprint (Astro-ph/9703175)
Castro-Tirado, A. J., et al. 1994, ApJS, 92, 469
Chakrabarti, S. K. 1996a, ApJ, 464, 664
————. 1996b, Phys. Rep., 266,229
Chakrabarti, S. K., & Titarchuk, L. G. 1995 ApJ, 455, 623
Ebisawa, K., Titarchuk, L., & Chakrabarti, S. K. 1996, PASJ, 48, 1
Eikenberry S. S., et al. 1998, ApJ, 494, L61
Frank, J., King, A. R., & Raine, D. J. 1985, Accretion Power in Astrophysics (Cambridge: Cambridge Univ. Press), 86
Greiner, J., Morgan, E. H., & Remillard, R. A. 1996, ApJ, 473, L107
————. 1998, New Astron. Rev., 42, 597-600
Laurent, P., & Titarchuk, L. 1999, ApJ, 511, L289
Lewin, W. H. G., van Paradijs, J., & Taam, R. E. 1995, in X-ray Binaries, eds. Lewin., W. H. G., J. van Paradijs, & E. P. J. van den Heuvel (Cambridge: Cambridge Univ. Press), 175

Mirabel, I. F., & Rodriguez, L. F. 1994, Nature, 371, 46
Mirabel, I. F., et al. 1998, A&A, 330, L9
Molteni, D., Sponholz, H., & Chakrabarti, S. K. 1996, ApJ, 457, 805
Narayan, R., Garcia, M. R., & McClintock, J. E. 1997a, ApJ, 478, L79
————. 1997b, ApJ, 482, 448
Narayan, R., Mahadevan, R, & Quataert, E. 1998, in Theory of Black Hole Accretion Disks, ed. M. A. Abramowicz, G. Bjornsson, & J. E. Pringle (Cambridge: Cambridge Univ. Press)
Narayan, R., & Yi, I. 1994, ApJ,428, L13
Orosz, J. A., & Bailyn, C. D. 1997, ApJ, 477, 876
Paul, B., et al. 1997, A&A, 320, L37
————. 1998a, A&AS, 128, 145
————. 1998b, ApJ 492, L63
Rao, A. R., et al. 1998, A&A, 330, 181
Shrader, C., & Titarchuk, L. 1998, ApJ, 499, L31
Taam, R. E., Chen, X., & Swank, J. H. 1997, ApJ, 485, L83
Tanaka, Y., & Lewin, W. H. G. 1995, in X-ray Binaries, ed. W. H. G. Lewin, J. van Paradijs, & E. P. J. van den Heuvel (Cambridge: Cambridge Univ. Press), 166
Titarchuk, L., & Zannias, T. 1998, ApJ, 493, 863